

This is a pre-print version of the paper: Analysis of particles size distributions in Mg(OH)₂ precipitation from highly concentrated MgCl₂ solutions. Submitted for publication to the Powder Technology.

Analysis of particles size distributions in Mg(OH)₂ precipitation from highly concentrated MgCl₂ solutions

G. Battaglia¹, S. Romano¹, A. Raponi², D. Marchisio², M. Ciofalo¹, A. Tamburini¹, A. Cipollina^{1}, G. Micale¹*

¹Università degli studi di Palermo, Dipartimento di Ingegneria, Viale delle Scienze, 90128 Palermo

²Department of Applied Science and Technology, Institute of Chemical Engineering, Politecnico di Torino, Torino, 10129, Italy

** corresponding author: andrea.cipollina@unipa.it*

Abstract

Magnesium is a raw material of great importance, which attracted increasing interest in the last years. A promising route is to recover magnesium in the form of Magnesium Hydroxide via precipitation from highly concentrated Mg²⁺ resources, e.g. industrial or natural brines and bitterns. Several production methods and characterization procedures have been presented in the literature reporting a broad variety of Mg(OH)₂ particle sizes. In the present work, a detailed experimental investigation is aiming to shed light on the characteristics of produced Mg(OH)₂ particles and their dependence upon the reacting conditions. To this purpose, two T-shaped mixers were employed to tune and control the degree of homogenization of reactants. Particles were analysed by laser static light scattering with and without an anti-agglomerant treatment based on ultrasounds and addition of a dispersant. Zeta potential measurements were also carried out to further assess Mg(OH)₂ suspension stability.

Keywords

Magnesium hydroxide; nanoparticles; mixing; precipitation; reactive crystallization; mineral recovery.

1. Introduction

The growing energy, water and raw materials demand is the challenge that humankind is facing every day. In the novel and promising concept of circular economy, what has always been a waste becomes a valuable resource to be re-used and valorised.

Since ancient times, table salt has been harvested from the sea through saltworks. The process leads also to highly concentrated mineral solutions (bitterns), free of calcium, as a by-product. Bitterns represent a treasure chest of some crucial elements, e.g. magnesium (Mg), lithium (Li) and other trace elements (TE) [1].

Magnesium concentration is typically of 1.1 to 1.7 g/L in seawater and it can reach a value up to 60 g/L in bitterns. The magnesium market has risen sharply in recent years and is foreseen to considerably grow in the future [2]. Magnesium has also been listed among the 30 Critical Raw Materials for the European Union, due to the geographical distribution of its producers, which are mainly located in the USA, China and Russia [3].

Magnesium is widely employed in the form of magnesium hydroxide ($\text{Mg}(\text{OH})_2$) and magnesium oxide (MgO). $\text{Mg}(\text{OH})_2$ and MgO belong to a group of compounds with large numbers of favourable properties and possible practical applications [4]. Magnesium hydroxide is used as a flame-retardant filler in composite materials as it undergoes endothermic dehydration at high temperature, as an acidic waste neutralizer, as a pharmaceutical excipient, as a preservative in the pulp and paper industry, as a fertiliser additive, as a component in ethanol chemical sensors and as the most important precursor for the preparation of magnesium oxide, which is largely employed as a catalyst [4,5]. $\text{Mg}(\text{OH})_2$ nanostructures have been obtained through several methods e.g. by microwave or ultrasonic/hydrothermal treatment [6,7], precipitation [1,8–12], precipitation with the aid of assistant additives [13], micro-emulsion method [14], bubbling set-up [15], hydrothermal process [16] and by means of a novel ionic exchange membrane crystallizer [17,18].

The recovery of magnesium from highly concentrated solutions represents a complex task. Turek et al. [11] successfully treated hard coal mine brine, which contained 2.84 g/L of magnesium, by extracting magnesium hydroxide through reactive precipitation. Cipollina et al. [1] produced high purity magnesium hydroxide from real bitterns collected from the saltworks operating in the district of Trapani (Italy). Yousefi et al. [10] synthesized magnesium hydroxide using poly(ethylene glycol, PEG 4000) as a surfactant; they applied a chemical precipitation method to an impure brine of the Khur Potash Complex's evaporation ponds (Isfahan, Iran). Vassallo et al. [19] presented a novel pilot plant for the selective recovery and removal of

magnesium and calcium from retentate brines of a nanofiltration unit processing spent brines from the industrial water production plant of Evides Industriewater B.V. More than 90% of magnesium ions contained in the treated brine were recovered with magnesium hydroxide purities above 90%.

The above-cited authors investigated some effects of operating conditions on the final magnesium hydroxide features, such as sedimentation times or solids purity. However, the authors did not study the interaction between mixing and precipitation (or reactive crystallization) occurring during the whole process, which, in fact, significantly affect the characteristics of the produced particles.

The reactive crystallisation process of $\text{Mg}(\text{OH})_2$ is a complex mix of phenomena, involving mixing at all scales, including at the molecular scale (i.e. micro-mixing), chemical reaction and homogeneous and heterogeneous nucleation, molecular growth, aggregation and agglomeration. As mentioned, in the case of very fast crystallization kinetics, mixing has a crucial role in the control of the final produced particle characteristics and notably the size distribution. Magnesium hydroxide production from a highly concentrated solution represents an example of an extremely fast crystallization process. Many studies dealt with the characterization of the crystallization kinetics of $\text{Mg}(\text{OH})_2$ [20–24]. Different experimental apparatuses were used, e.g. T-mixers [20] or stirred reactors [21,22]; the induction time (the period of time that elapses between the moment when supersaturated solutions are formed and the moment when precipitate appears) was found to be at most of the order of few seconds even when the magnesium concentration was as low as ~ 0.03 g/L [22].

Only a few works addressed the effect of mixing on the magnesium hydroxide precipitation processes from concentrated solutions. Shirure et al. [25] investigated the precipitation of magnesium hydroxide from magnesium chloride solutions (up to 24 g/L) using narrow channels T and Y- shaped mixers. The authors reported that at higher reactant flow rates, smaller $\text{Mg}(\text{OH})_2$ particles were produced. The surfactant Tween 20 was added to the $\text{Mg}(\text{OH})_2$ suspensions before particle size distributions (PSDs) measurements and the volume-average particle size was found to be from 5 μm to 30 μm . Song et al. [26] synthesized magnesium hydroxide particles with high purity by using MgCl_2 solutions (~ 40 g/L) and NaCl solution as assistant additive, in a glass reactor under vigorous stirring. In this case, PSDs were measured by static light scattering granulometry analysis without using surfactants and particles of the order of micrometres were reported. In addition, significant aggregate/agglomerates were observed by SEM images. Tai et al. [27] studied the precipitation

of magnesium hydroxide nanoparticles from highly concentrated magnesium chloride solutions (up to 20 g/L) using a spinning disk reactor. The spinning disk reactor allowed a very good degree of mixing (a mixing time below 1 ms) leading to the synthesis of lamellar magnesium hydroxide particles of 50-80 nm length and 10 nm in thickness. In this case, the authors used a sonicator and poly(acrylic acid, sodium salt) (PAA) and sodium hexametaphosphate as dispersants. Particles were measured using a dynamic light scattering technology yielding number-average particle size from 40.0 to 47.5 nm. Shen et al [28] developed a novel impinging stream-rotating packed bed reactor. In order to determine the particle size and distribution, the prepared samples were dispersed in distilled water by sonication for 10 min using a 2% sodium hexametaphosphate solution as a dispersant. Wide size distributions were found at low liquid flow rates and rotating packed bed speed, while PSDs narrowed when the liquid flow rates and the rotating packed bed speed increased (e.g. the increase of the fluid flow rate of a Mg^{2+} 18 g/L solution yielded a decrease of the volume-average size from 104 to 58.4 nm when the rotating packed bed velocity was 800 rpm).

The broad dispersed $Mg(OH)_2$ particle dimensions reported in the above-cited works mark the need for a deeper insight into the phenomena taking place during $Mg(OH)_2$ precipitation, including the un-doubtful interaction between precipitation and mixing, the effect of ultrasounds and/or dispersant addition. To this aim, a comprehensive experimental study is here presented on the interaction between reactants mixing and $Mg(OH)_2$ precipitation from highly concentrated synthetic $MgCl_2$ solutions (Mg^{2+} 24 g/L). Two circular cross-sectional T-shaped mixers, having a diameter of 2 mm or 3 mm, were employed to tune and control the degree of reactants homogenization. PSDs were accessed using static light scattering technique, with and without ultrasounds treatment and addition of PAA as a dispersant. Also zeta potential measurements were conducted at different pH values in order to better investigate the tendency of particles to agglomerate.

To describe the state of particle assemblage, unfortunately, a broad disagreement is observed among different authors and sources on the definition of terms “agglomerates” and “aggregates” [29]. In the present paper the following definitions will be used:

- primary particles are single crystals or crystals composed of crystallites (or grain);
- aggregates are made of primary particles, which are united by strong chemical bonds that cannot be broken by fluid shear stresses and sonication;
- agglomerates are made of more or less loose arrangements of primary particles, aggregates or a mixture of the two held together by crystalline bridges or sometimes

by electrostatic forces. Agglomerates are weaker than aggregates and can be separated by physical treatment such as sonication.

2. Materials and methods

2.1 Reactive crystallization stage

2.1.1 Experimental set up and $Mg(OH)_2$ reaction

A schematic representation of the employed experimental set-up is shown in **Figure 1**. Magnesium hydroxide precipitation was carried out employing two circular-cross sectional T-mixers with a diameter of 2 and 3 mm, as shown in the insight of Figure 1. The T-mixers were drilled in polymethyl methacrylate (PMMA) blocks and are constituted by two horizontal tracts (inlet channels) which merge into a vertical one (mixing channel). In both mixers, the inlet and mixing channels were of the same diameter (2 mm for mixer A and 3 mm for mixer B). The inlet channels were 10 times longer than the mixer diameter, i.e. 20 and 30 mm for mixers A and B, while the vertical channels were twenty times longer than the mixer diameter, i.e. 40 and 60 mm, respectively. The two T-mixers were employed to investigate the effect of mixing performance in the reactors on the precipitated $Mg(OH)_2$ particles. In particular, it is expected that narrower channels offer better mixing performance with respect to larger ones [30]. Magnesium chloride ($MgCl_2$) and sodium hydroxide ($NaOH$) solutions were pumped using two gear pumps (Fluid-o-Tech® FG series) controlled by dedicated software developed on LabView 2015.

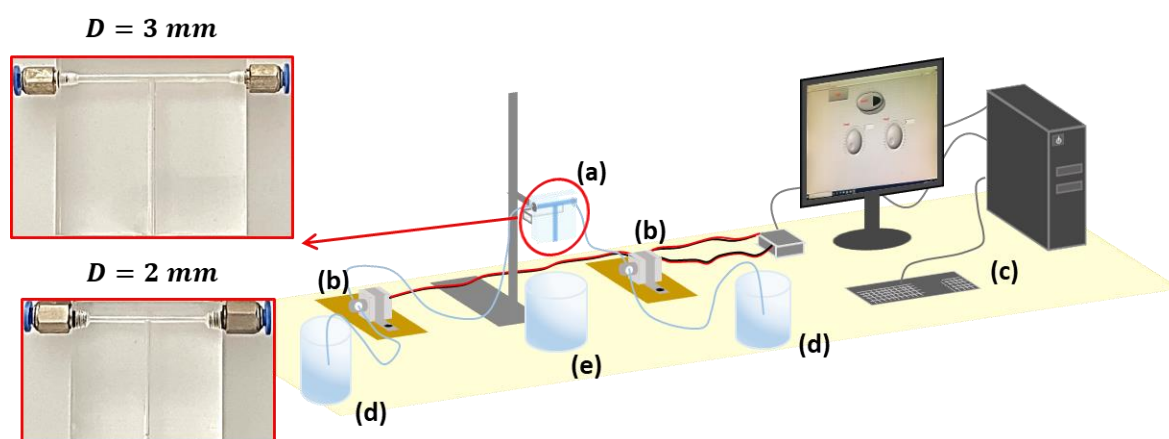
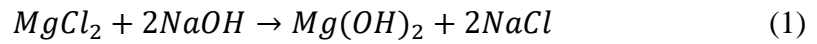


Figure 1 Schematic representation of the employed experimental set-up: (a) T-mixer, (b) gear pumps, (c) computer for pumps control, (d) feed tanks, (e) discharge tank. On the left, an insight of the 3 and 2 mm T-mixers.

Gear pumps are typically used for industrial applications, since they can be operated continuously, however they are not pulsation-free. The majority of the experiments reported here were conducted at high pump rotational speed, thus the effect of pulsation on the mixing of the reactants is expected to be negligible [31].

The chemical reaction involved in the formation of magnesium hydroxide is:



MgCl₂ and NaOH solutions were prepared by dissolving pellets of magnesium chloride hexahydrate for analysis (Sigma Aldrich) and NaOH (Honeywell Fluka™, with an assay > 98%) in ultrapure water. MgCl₂ concentrations were verified by Ionic Chromatography (Metrohm 882 compact IC plus), while NaOH concentrations were measured by titration. All solutions were prepared with an error in target concentration lower than 3% with respect to the desired values.

2.1.2 Flow rates and estimation of the characteristic mixing times

To design and scale-up precipitation reactors, it is important to estimate the mixing efficiencies and the characteristic mixing time attained in the employed T-mixers. T-mixers are characterized by large area-to-volume ratio providing better mixing efficiencies with respect to conventional reactors (e.g. stirred reactors). In the last decades, T-mixers have been thoroughly investigated both experimentally [31,32] and numerically [30,33]. The characteristic mixing time (t_m) in such mixers depends on the specific definition adopted. However, an estimate is provided by Roelands et al. [30]:

$$t_m = \frac{12D}{v} \quad (2)$$

where D is the diameter of the vertical channel and v is the mean velocity in the same channel.

The effect of reactants homogenization, and thus of mixing time, on the precipitation of Mg(OH)₂ was investigated here at different fluid velocities in the mixing channel: from 0.6±2% to 6.4±2% m/s in the T-mixer of 3 mm diameter (mixing times between ~60 ms and ~6 ms); and from 4.1±2% to 17±2% m/s in the 2 mm diameter mixer (mixing times between ~6 ms and ~1 ms).

Table 1 lists all the cases investigated along with the flow rates, the mean velocity, the Reynolds number in the vertical channel and the estimation of the characteristic mixing times calculated using Eq. (2). In all cases, a 1M MgCl₂ solution, a typical concentration of bitterns, was made to react with a stoichiometric 2M solution of NaOH. MgCl₂ and NaOH solutions

were fed at the same fluid flow rates, each half of the flow rate in the mixing channel. All tests were conducted at 25°C.

Table 1 Geometrical and operating conditions of experimental tests. In all cases a 1M MgCl₂ solution was made to react with a stoichiometric 2M solution of NaOH. The flow rates, the mean velocity and the Reynolds numbers are calculated in the mixing channel.

Case	Mixer Diameter <i>D</i> (mm)	Flow rate (mL/min)	Mean velocity <i>v</i> (m/s)	Reynolds number	Estimated mixing time (ms)
#1	3	260 ± 2%	0.6 ± 2%	2030	60
#2	3	460 ± 2%	1.1 ± 2%	3590	33
#3	3	1400 ± 2%	3.3 ± 2%	10970	10
#4	3	2720 ± 2%	6.4 ± 2%	21300	5.6
#5	2	780 ± 2%	4.1 ± 2%	9170	5.7
#6	2	1600 ± 2%	8.5 ± 2%	18830	2.9
#7	2	2320 ± 2%	12 ± 2%	27250	2.0
#8	2	3203 ± 2%	17 ± 2%	37660	1.4

The Reynolds number was calculated as follows:

$$Re = \frac{\rho v D}{\mu} \quad (3)$$

where ρ and μ are the density and the viscosity of pure water at 25°C (997 kg/m³ and 0.89 · 10⁻³ Pa·s, respectively), v is the mean fluid velocity in the vertical (mixing) channel and D is the channel diameter. The range of the investigated flow rates results in a range of Reynolds numbers from 2,000 to 38,000.

The suspensions' pH was measured immediately after the outlet of the mixing channel. In all tests here presented, the measured pH values ranged between 10.3 and 10.6 (equilibrium pH of 10.48).

2.2 Product characterization stage

2.2.1 Particle Size distribution measurements

Mg(OH)₂ particle size distributions (PSDs) were measured using a Malvern® Mastersizer 2000 granulometer with and without ultrasounds treatment and addition of a poly(acrylic acid, sodium salt), (PAA, MW 1200, Sigma-Aldrich, Inc.) as a dispersant.

The Mastersizer 2000 is a static light scattering equipment that uses a blue (488.0 μm wavelength LED) and red (633.8 μm wavelength He-Ne laser) light dual-wavelength, single-lens detection system. The light intensity adsorbed by particles is measured as obscuration and refers to the amount of the analysed sample. PSDs are obtained by processing light scattering

data using the Malvern's Mastersizer 2000 software that employs either full Mie or Fraunhofer diffraction theories [34].

The granulometer was equipped with the Malvern® Hydro 2000 MU that uses a stirrer for the dispersion of the sample into ~800 mL of deionised water. All the analyses were carried out at stirrer velocity of 2000 rpm. This stirrer velocity was deemed to be the one that did not affect the obtained particle size distributions, after performing a preliminary stirrer speed influence study on PSDs as suggested in the literature [34–36]. Most Mastersizer2000 measurements were carried out as follows: (1) the PAA (when adopted) was added to water in the Hydro 2000 MU beaker (30 PAA drops for ~5mL of Mg(OH)₂ 29.3 g/L suspension) and the background was measured; (2) the Mg(OH)₂ suspension was added until the light obscuration reached a value of ~24%; (3) at least 5 PSD measurements were conducted; (4) 5 minutes of ultrasounds treatment (sonication) were performed using the integrated ultrasound probe at 20 kHz; (5) at least 5 further PSD measurements were taken. For comparison purposes, some PSD measurements were also conducted without either PAA or sonication. All Mg(OH)₂ samples were analysed within less than 15 minutes from their precipitation.

The effect of time delay in performing the analysis on the Mg(OH)₂ precipitation was investigated by quenching Mg(OH)₂ precipitates obtained from initial 0.1M MgCl₂ and 0.2M NaOH solutions. Specifically, the suspension exiting the T-mixer was quenched in a flask containing ultrapure water leading to a product dilution of 1:2 and 1:10. The collected solutions were then analysed by ionic chromatography to determine the final concentration of Mg²⁺ ions and thus Mg²⁺ conversion. In all cases, a total Mg²⁺ conversion was found suggesting that the reaction fully developed in the T-mixer; therefore, no effect (or a very low effect) of nucleation, particle growth and aggregation was expected after the solution exited the T-mixer. This is justified by the fact that supersaturation was already consumed even at these low concentrations, lower than those used in the actual tests (Table 1). Each experiment was repeated at least twice for the purpose of reproducibility.

2.2.2 Zeta potential measurements

In order to better understand the stability of Mg(OH)₂ colloids (the ability to stay in the colloidal form without particle agglomeration through flocculation [37]) and its implications on the obtained PSD, zeta potential measurements were conducted analysing Mg(OH)₂ suspensions produced: (i) after 2 hours from the precipitation; (ii) after 1 month of aging. The 2 hours samples were analysed using a Malvern® Zetasizer Nano SP (analysis conducted at

the Advanced Technologies Network Center of the University of Palermo), while the 1 month samples were analysed using a Malvern® Zetasizer Nano ZS90 (analysis conducted at Politecnico di Torino). All samples were diluted to a Mg(OH)₂ concentration of 0.3 g/L and drops of 1M NaOH solution were added to adjust the suspensions pH to the desired one. No PAA was used. Each experiment was repeated at least twice for the purpose of reproducibility.

2.2.3 SEM analysis

The morphology of the Mg(OH)₂ particles produced for Case #7 was analysed by Scanning Electron Microscope (SEM FEI Quanta 200 FEG). Mg(OH)₂ suspensions were filtered by using a Büchner system and a vacuum pump. The cake was washed to remove the reaction produced NaCl that remains trapped in the wet cake, and then dried for 24h in an oven at 120°C.

3. Results and Discussion

3.1 Influence of the reactants mixing on the produced Mg(OH)₂ particles

In this section, the influence of mixing on the produced Mg(OH)₂ particles was assessed by comparing the PSDs obtained for the eight experimental conditions reported in **Table 1**. For the chosen concentrations of 1M MgCl₂ and 2M NaOH the minimum degree of mixing (the highest mixing time, see Eq. (2)) beyond which mixing has no further influence on particle formation was determined. As discussed in Section 2, PSDs were measured with and without ultrasounds treatment and addition of PAA in the characterization stage in order to assess the Mg(OH)₂ particle assemblage state.

3.1.1 Mg(OH)₂ PSDs without ultrasounds treatment and no addition of PAA

PSDs measurements were first performed without ultrasounds treatment and addition of PAA. The characteristic diameters dkm of the measured PSDs were calculated to study the effect of fluid flow regimes on the Mg(OH)₂ precipitation process. dkm denotes the ratio between the k -th and the m -th moments of the PSD:

$$dkm = \left[\frac{\int_0^{\infty} d^k n(d) dd}{\int_0^{\infty} d^m n(d) dd} \right]^{\frac{1}{k-m}} \quad (4)$$

where $n(d)$ is the number particle distribution function, such that $n(d)dd$ is the number of particles having diameter between d and $d + dd$. Thus, d_{10} is the number-average particle size more affected by small particles as they outnumber larger ones. Instead, d_{43} is the volume

weighted-average particle size, which is more influenced by the presence of larger particles [38]. **Figure 2** reports the d_{43} and d_{10} characteristic diameters of the PSDs of the obtained $\text{Mg}(\text{OH})_2$ precipitate for all the fluid flow regimes investigated.

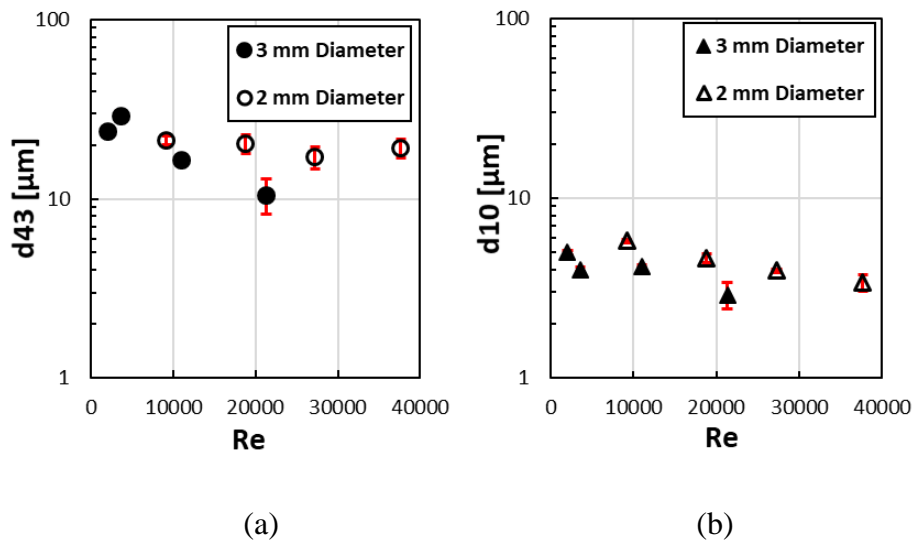


Figure 2 Characteristic diameters of $\text{Mg}(\text{OH})_2$ particles obtained using T-mixers with a diameter of 3 mm (solid symbols) or 2 mm (hollow symbols) as a functions of Reynolds number: a) d_{43} ; b) d_{10} . No sonication or PAA treatment was performed.

As can be seen in **Figure 2**, neither d_{43} nor d_{10} exhibit a slightly influence of the Reynolds number or the diameter of the T-mixers. In particular, d_{43} decreases from 30 to 10 μm when the 3 mm diameter T-mixer is used (solid symbols in **Figure 2.a**), while it fluctuates around 20 μm in the case of the 2 mm diameter T-mixer (hollow symbols in **Figure 2.a**). d_{10} decreases from ~6 μm to ~3 μm when the flow rate increases in both mixers (**Figure 2.b**). These results were somehow un-expected, as in previous works the characteristic dimension of the particles was reported to decrease and PSDs to become more narrow as the mixing of reactants increased, as in the case of barium sulphate [38–40].

For the sake of completeness, volume-particle size distribution (V-PSD) of all the investigated Cases are also illustrated in **Figure 3**. In particular, V-PSD reports the quantity $\varphi(d)$, which is the volume particle distribution function normalized by the total volume of particles, such that $\varphi(d)dd$ is the volume percent of particles having diameters between d and $d + dd$.

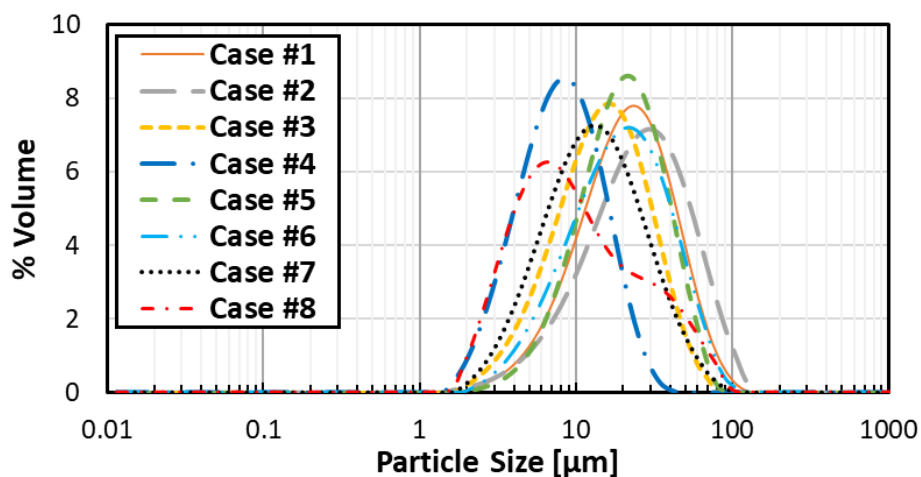


Figure 3 Volume particle size distributions for all the investigated Cases. No sonication or PAA treatment was performed. Cases #1-4 are obtained in the 3 mm diameter T-mixer, while cases #5-8 in the 2 mm diameter (Table 1).

V-PSDs show a rather random influence either of mixing reactants flow rate or T-mixer diameter. The obtained $Mg(OH)_2$ V-PSDs are of the same order of particle dimensions with respect to those reported by Song et al. [26] and Shirure et al. [25]. Note that also the latter authors produced $Mg(OH)_2$ and did not treat particles with ultrasounds and adding dispersants (see further remarks at the end of Section 3.2).

3.1.2 $Mg(OH)_2$ particle size distributions with PAA and ultrasounds

Particle size distributions were also investigated after ultrasounds treatment and the addition of PAA. The use of PAA was used by several other authors [37,41,42]. **Figure 4** reports the obtained d_{43} and d_{10} for the same cases of **Figure 2**.

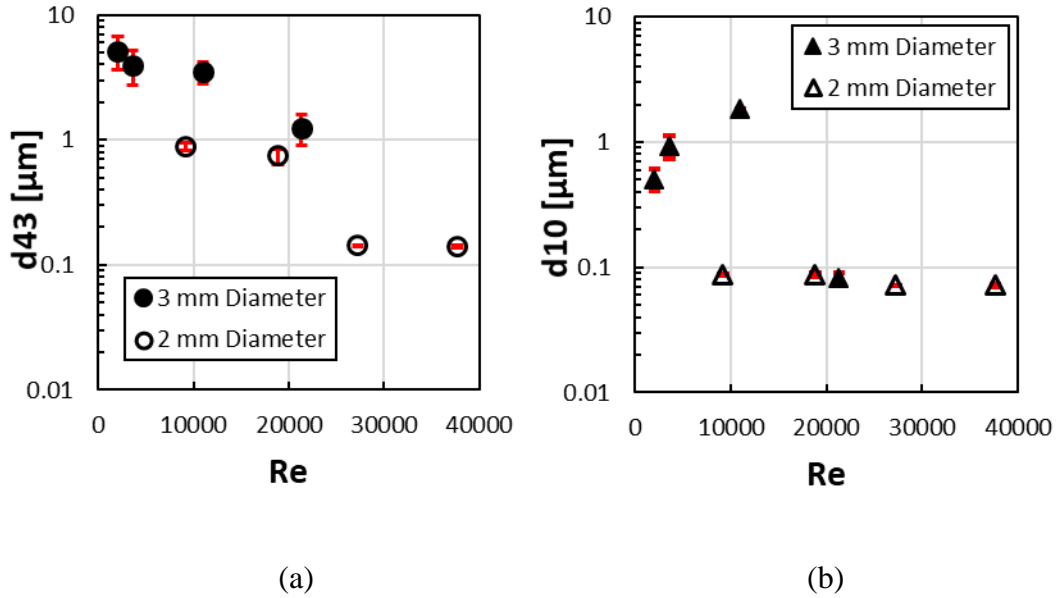


Figure 4 Characteristic diameters of $Mg(OH)_2$ particles obtained using T-mixers with a 3 mm (solid symbols) or 2 mm (hollow symbols) as a functions of the Reynolds number: a) d_{43} ; b) d_{10} . PSDs were obtained after 5 minutes of ultrasounds treatment and using PAA as a dispersant.

Particle sizes significantly differ from those reported in **Figure 2** and a stronger, although still irregular, influence of mixing parameters (velocity and diameters) on the characteristic particle diameters can be now observed. In particular, d_{43} (**Figure 4.a**) decreases from $\sim 5 \mu m$ to $\sim 1 \mu m$ when the Reynolds number increases from $\sim 2,000$ to $\sim 20,000$ in the 3mm diameter T-mixer. Lower d_{43} values are observed for all the fluid flow rates when the 2 mm diameter T-mixer is employed, indicating a better mixing quality. Specifically, d_{43} values decrease from $\sim 1 \mu m$ at Re of $\sim 10,000$ to $\sim 0.1 \mu m$ at Re of $\sim 27,000$ - $38,000$ (Cases #7 and #8). In the 3 mm diameter T-mixer, d_{10} (**Figure 4.b**) increases for Reynolds numbers $< 10,000$, while it suddenly drops at the investigated highest Reynolds value (i.e. $\sim 20,000$). The 2 mm diameter T-mixer guarantees better mixing quality as d_{10} exhibits low values even at the lowest fluid flow rate and settles at $\sim 0.08 \mu m$ at Reynolds number of $\sim 27,000$ - $38,000$ (Case #7 and #8).

The volume-PSDs for all Cases are shown in **Figure 5**.

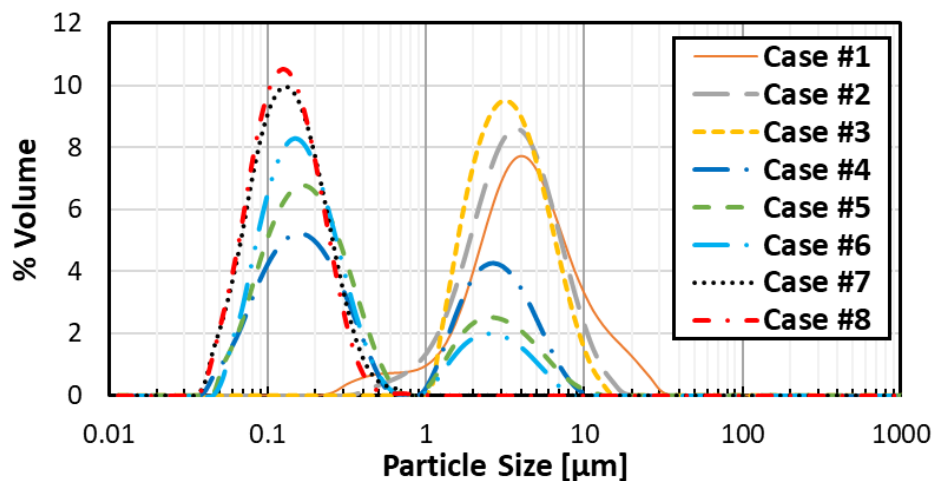


Figure 5 Volume particle size distributions for all the investigated Cases. V-PSDs were obtained after 5 minutes of ultrasounds treatment and using PAA as a dispersant. Cases #1-4 are obtained in the 3 mm diameter T-mixer, while cases #5-8 in the 2 mm diameter (Table 1).

From Case #4 to Case #6, i.e. for intermediate mixing intensities (mixing times between 6 and 3 ms), V-PSDs are bi-modal distributions with two peaks, one at $\sim 2.7 \mu\text{m}$ for coarse particles and another at $\sim 0.13 \mu\text{m}$ for fine particles. Such bi-modal distributions are typical of *shattering*, probably caused by the use of ultrasounds, by which large agglomerates are broken into aggregates (the fine particles having peak size $\sim 0.13 \mu\text{m}$) and smaller agglomerates (exhibiting a peak size of $\sim 2.7 \mu\text{m}$) [43]. The total volume of larger agglomerates decreases, and the total volume of the smaller aggregates increases as mixing increases, while peak particle sizes remain almost the same. On the other hand, from Case #1 to Case #3 (high mixing times ranging from 60 to 10 ms), V-PSDs indicate a unimodal distribution with the presence of mainly coarse particles, whose size is 2-3 times smaller than those shown in **Figure 3**. Finally, at the highest mixing rate (mixing time values lower than 2 ms), Cases #7 and #8, particles are again monodispersed exhibiting only one peak at $\sim 0.13 \mu\text{m}$, characteristic of $\text{Mg}(\text{OH})_2$ aggregates. It should be worth to recall that, in the present work, the term aggregates refers to primary particles, which are made of crystals united by strong chemical bonds and cannot be broken by fluid shear stresses and sonication. On the other side, the term agglomerates refers to looser or stronger arrangements of primary particles, aggregates, or a mixture of the two, held together by crystalline bridges or sometimes by electrostatic forces. Agglomerates are weaker than aggregates and can be separated by physical treatment such as sonication.

A possible explanation of the behaviour exhibited by the above discussed results lies in the interaction between mixing and the numerous phenomena involved in the precipitation

process, as discussed by many authors [44,45]. Larger particles are produced in the reactive stage when mixing is poor (high mixing times) due to the combination of (1) a low homogenization degree of the reactants, yielding high local supersaturation levels, and (2) large and long-lived Kolmogorov eddies, which can enclose a high number of particles that can remain close to one another enough time to establish strong bridges between them. These bridges cannot be broken by the low fluid shear stresses. Conversely, at high Reynolds numbers, mixing becomes more efficient (low mixing times); more homogenous supersaturation is attained; small and short-lived Kolmogorov eddies are formed, so that a lower number of particles are entrapped inside each eddy, and stay together for a shorter time. These particles could form either small aggregates or weak agglomerates, the latter characterized by bridges which could be broken by the high fluid shear stresses.

For the presented results (**Figure 5**), it can be stated that a mixing time of at most 2 ms (Cases #7 and #8) must be achieved inside the reactor in order to well homogenize highly concentrated MgCl_2 (1M) and NaOH (2M) solutions. As a matter of fact, $\text{Mg}(\text{OH})_2$ nanoparticles produced for Cases #7 and #8 (mixing times lower than ~ 2 ms) are characterized by aggregates or weak agglomerates, the latter breakable by the use of ultrasounds, leading to aggregates of ~ 100 - 200 nm after sonication. On the contrary, $\text{Mg}(\text{OH})_2$ nanoparticles produced for Cases #1-3 (mixing times between 60-10 ms) are characterized by strong agglomerates, which require high energy to be broken into aggregates, thus exhibiting V-PSDs of micrometre sized agglomerates after 5 minutes of sonication. The intermediate mixing rates of Cases #4-6 (mixing times between ~ 6 ms and ~ 3 ms), instead, consist of a mix of strong and weak agglomerates, which can be partially broken to aggregates by ultrasounds leading to a bi-modal distribution characterized by aggregates of ~ 100 - 200 nm and agglomerates having a peak size of ~ 2.7 μm .

The importance of mixing time as controlling phenomena is also confirmed by the fact that suspensions produced using different T-mixers (3 and 2 mm diameter for Case #4 and Case#5) and flow rates (2720 and 780 mL/min for Case #4 and Case #5), but having similar mixing times (~ 6 ms) exhibit similar V-PSDs (see **Figure 5**) and particle size dimensions (**Figure 4**).

$\text{Mg}(\text{OH})_2$ nanoparticles obtained for Case #7 and 8 at a mixing time lower than ~ 2 ms have comparable particle dimensions with those reported by Tai et al. [27], i.e. $d_{10} \sim 60$ nm, who also produced $\text{Mg}(\text{OH})_2$ nanoparticles starting from 1M MgCl_2 employing a spinning disk reactor where the mixing time was reported to be of ~ 1 ms.

3.2 Zeta Potential measurements

In Section 3.1 it was shown that particle size distributions significantly vary when suspensions are treated by using ultrasounds and adding PAA as a dispersant. In order to better understand these results, the effect of superficial electric charge of $\text{Mg}(\text{OH})_2$ particles was examined by performing Zeta-potential measurements. The stability of $\text{Mg}(\text{OH})_2$ suspensions was also investigated over time performing the analysis (i) after 2 hours and (ii) after 1 month of aging from the precipitation. Zeta-potential depends on the particle properties, the suspension conditions (e.g. pH), and the theoretical model applied, e.g. the Smoluchowski approximation employed here to derive Zeta-potential values from the electrophoretic mobility of particles [46]. **Figure 6** presents Zeta-potential values measured for Case #7 (see **Table 1**), as described in section 2.2.2, for suspension pH ranging from 10 to 13.

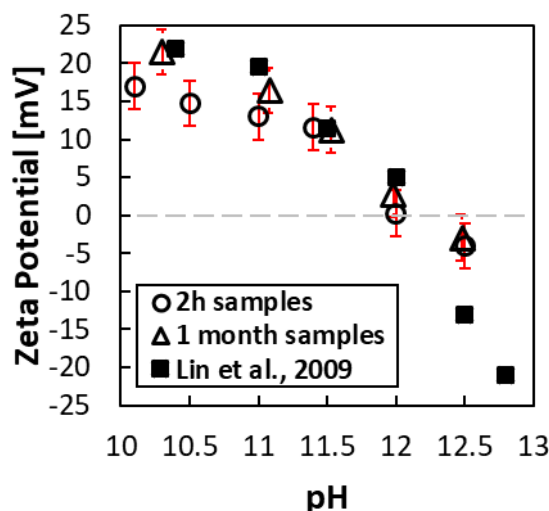


Figure 6 $\text{Mg}(\text{OH})_2$ Zeta potential as a function of suspension pH. Hollow circle and triangle symbols refer to the same $\text{Mg}(\text{OH})_2$ suspension analysed: (i) 2 hours after the precipitation (circles) and (ii) after 1 month of aging (triangles). Lin et al. data were taken from [47].

The experimental data collected in this study was compared with those presented by Lin et al. [47]. The latter authors employed an electro-acoustic technique, while the data reported here were obtained by means of Malvern® Zetasizers, which are based on the electrophoretic mobility technique, i.e. on measuring the limiting velocity of the particles in an electric field.

At solution pH between 10 and 11, a fair agreement is observed between Lin et al. data and Zeta-potential values measured analysing the 2 hours samples. On the contrary, aged samples showed a better agreement with Lin et al. measurements.

Specifically, Zeta-potential values measured for the 2 hours samples were found to vary from ~ 18 mV to ~ 13 mV, while Zeta-potential values reported by Lin et al. and those measured for the aged samples decreased from ~ 23 mV to ~ 17 mV. Some difficulties were encountered for measurements in high pH suspensions due to their high conductivity values, so that pH values higher than 12.5 could not be investigated. Lin et al, however, reported Zeta-potential values of ~ -15 mV at pH ~ 12.5 and ~ -20 mV at pH ~ 13 . The isoelectric point (the point of zero Zeta-potential, where colloids have the largest tendency to agglomerate) of $\text{Mg}(\text{OH})_2$ particles is detected at a pH value of ~ 12 for both 2h samples and aged samples, in good agreement with Lin et al. and with values reported in literature [42,48,49].

Zeta-potential values measured for samples produced after 2 hours from precipitation and those aged for 1 month show that $\text{Mg}(\text{OH})_2$ suspensions are characterized by the same stability characteristics over time. In particular, from **Figure 6**, it can be clearly seen that the Zeta-potential of the $\text{Mg}(\text{OH})_2$ particles lies in the range of ± 30 mV, which represents a zeta potential region where particles are not stable and tend to agglomerate rather than staying apart [46]. These Zeta-potential values explain the behaviour shown in Section 3.1. Specifically, in the absence of PAA, $\text{Mg}(\text{OH})_2$ particles agglomerate due to their low zeta potential values. On the other hand, the presence of PAA stabilizes the $\text{Mg}(\text{OH})_2$ suspension [37,41]. The thermodynamically stable coiled structure of PA^- can entrap $\text{Mg}(\text{OH})_2$ nanoparticles preventing their agglomeration [37]. Thus, V-PSDs obtained in the absence of sonication and no PAA addition, as in **Figure 3**, do not exhibit a significant influence of mixing in the reactive crystallization stage because they mainly regard the size distribution of large and weak agglomerates with typical peak dimensions in the 8-20 μm range. On the contrary, V-PSDs obtained by applying sonication and PAA treatment (**Figure 5**) exhibit a much larger influence of the mixing intensity experienced in the reactive crystallization stage; for low mixing, V-PSDs exhibit agglomerates smaller than those in Figure 3, but still characterized by peak size of 2-3 μm , while, for high mixing, they only consist of aggregates with a typical size of 100-200 nm.

3.3 Tyndall effect and $\text{Mg}(\text{OH})_2$ particles morphology

The reduction of the particles sizes presented in **Figure 4** with respect to those reported in **Figure 3** was also confirmed by a visual inspection of the $\text{Mg}(\text{OH})_2$ suspension contained in the Hydro 2000 MU beaker, as shown in **Figure 7** for Case #7 and Case #8.

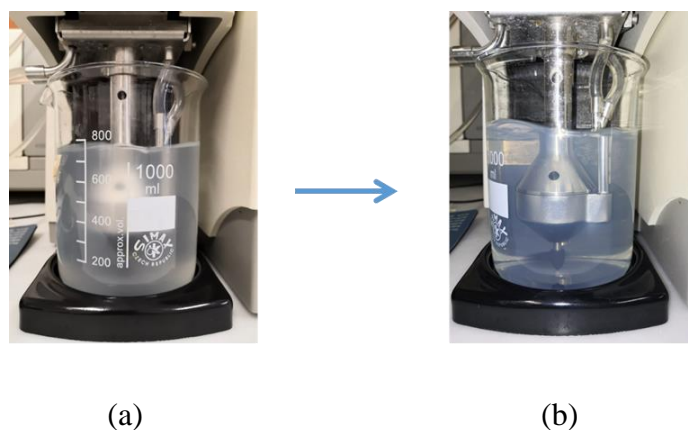
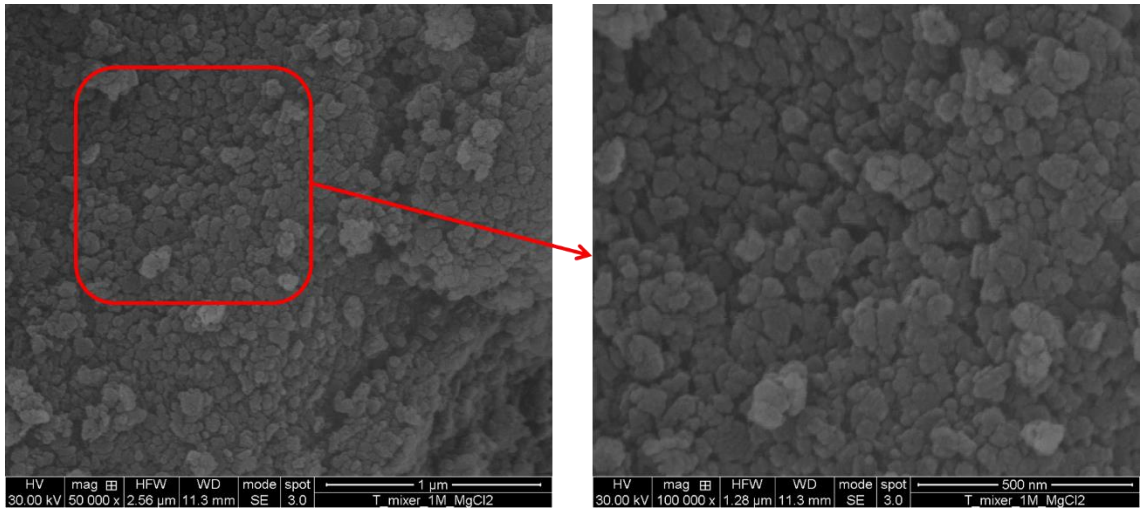


Figure 7 $Mg(OH)_2$ suspensions in the Malvern® Hydro 2000 MU beaker before (a) and after (b) applying ultrasounds in the presence of PAA for Case #7 and Case #8. The blueish colour of the suspension after the anti-agglomerant treatment (b) indicates the presence of particles with dimensions below ~ 900 nm (Tyndall effect).

The $Mg(OH)_2$ suspension changes from a whitish to a blue colour due to the Tyndall effect. The Tyndall effect occurs when light is scattered by particles with diameters below ~ 900 nm [50], demonstrating the presence of nanometre sized particles in the beaker. Contrariwise, suspensions of particles produced under conditions #1-6 did not exhibit Tyndall effect due to the fact that the presence of large particles dominate and mask the effect of small particles. Note that, when measuring nanometre $Mg(OH)_2$ particles, the absorption value of $Mg(OH)_2$ was changed from 0.1 to 0.

As far as the morphology of the $Mg(OH)_2$ particles is concerned, **Figure 8** presents SEM images at two increasing magnifications (1 μm and 500 nm) of the produced $Mg(OH)_2$ particles obtained following the procedure described in Section 2.2.3. $Mg(OH)_2$ globular nanometre particles with characteristic sizes of ~ 50 -200 nm can be observed with a low tendency to form platelet-like nanoparticles. Similar particles morphologies were also reported in literature for $Mg(OH)_2$ particles produced by precipitation using $MgCl_2$ solutions [42,51].



(a)

(b)

Figure 8 SEM image of the produced particles for Case #7 at a magnification of (a) 1 μm and (b) 500 nm.

Conclusions

The precipitation process of magnesium hydroxide from 1M MgCl₂ solutions was experimentally investigated focusing on the effect of reactants mixing on particle size distribution by a clearly methodical analytical procedure for the characterization of the produced Mg(OH)₂ particles. Two circular cross-sectional T-shaped mixers of 2 and 3 mm diameter were employed. Eight different cases were investigated with variable flow rates and channel diameter, in the range of Reynolds numbers between 2,000 and 38,000, thus leading to mixing times ranging from 60 to 1.5 ms. Produced particles were analysed via a light scattering technique within 15 mins from precipitation, with and without sonication (ultrasounds treatment) and poly(acrylic acid sodium salt) (PAA) addition.

It was found that in the absence of PAA and ultrasounds treatment particles could not be well characterized since similar V-PSDs exhibiting large agglomerates with peak sizes of 8-20 μm were detected for all the cases investigated. On the contrary, by using PAA and sonication, the effect of reactants mixing was clearly shown and the particles assemblage state well characterized. Specifically, for intermediate mixing regimes, V-PSDs were found to be bimodal with two peaks, one at ~2.7 μm characteristic of small Mg(OH)₂ agglomerates and another at ~0.13 μm characteristic of Mg(OH)₂ aggregates. At low mixing rates, V-PSDs indicated a unimodal distribution with the presence of only agglomerates exhibiting a peak of ~2.7 μm, while at the highest mixing, when mixing time reaches values below 2 ms, particles were again monodispersed, exhibiting only one peak size of ~0.13 μm, representative of Mg(OH)₂ aggregates.

The similar V-PSDs obtained without any particle treatment were consistent with the low measured zeta potential values of the Mg(OH)₂ particles, which were found to lie in the range of ±30 mV, marking a high tendency of particles to agglomerate due to electrostatic forces.

Acknowledgments

This project has received funding from the European Union's Horizon 2020 research and innovation programme under Grant Agreement No. 869467 (SEArcularMINE). This output reflects only the author's view. The European Health and Digital Executive Agency (HaDEA) and the European Commission cannot be held responsible for any use that may be made of the information contained therein. Authors are grateful to Simone Bonafede for having contributed to this work during his master thesis.

Author statement

Giuseppe Battaglia: Conceptualization, Methodology, Formal analysis, Data curation, Validation, Investigation, Writing - Original Draft, Visualisation.

Salvatore Romano: Conceptualization, Methodology, Formal analysis, Data curation, Validation, Investigation, Writing – Review & Editing, Visualisation.

Antonello Raponi: Conceptualization, Methodology, Investigation.

Daniele Marchisio: Conceptualization, Methodology, Supervision, Writing – Review & Editing, Project administration.

Michele Ciofalo: Methodology, Formal analysis, Writing – Review & Editing.

Andrea Cipollina: Conceptualization, Methodology, Writing – Review & Editing, Supervision, Project administration, Funding acquisition.

Alessandro Tamburini: Methodology, Formal analysis, Resources, Supervision.

Giorgio Micale: Conceptualization, Resources, Supervision, Project administration, Funding acquisition.

Declaration of Competing Interest

The authors declare that they have no known competing financial interests or personal relationships that could have appeared to influence the work reported in this paper.

References

- [1] A. Cipollina, M. Bevacqua, P. Dolcimascolo, A. Tamburini, A. Brucato, H. Glade, L. Buether, G. Micale, Reactive crystallisation process for magnesium recovery from concentrated brines, *Desalin. Water Treat.* 55 (2015) 2377–2388. <https://doi.org/10.1080/19443994.2014.947771>.
- [2] Magnesium Metal Outlook to 2030, 13th Edition, (2021) 1–7. <https://roskill.com/market-report/magnesium-metal/>.
- [3] Critical Raw Materials Resilience: Charting a Path towards greater Security and Sustainability, (2020). <https://eur-lex.europa.eu/legal-content/EN/TXT/PDF/?uri=CELEX:52020DC0474&from=EN>.
- [4] A.A. Pilarska, Ł. Klapiszewski, T. Jesionowski, Recent development in the synthesis, modification and application of Mg(OH)₂ and MgO: A review, *Powder Technol.* 319 (2017) 373–407. <https://doi.org/10.1016/j.powtec.2017.07.009>.
- [5] G. Balducci, L. Bravo Diaz, D.H. Gregory, Recent progress in the synthesis of nanostructured magnesium hydroxide, Royal Society of Chemistry, 2017. <https://doi.org/10.1039/c7ce01570d>.

- [6] H.Y. Zahran, S.S. Shneouda, I.S. Yahia, F. El-Tantawy, Facile and rapid synthesis of nanoplates Mg(OH)₂ and MgO via Microwave technique from metal source: structural, optical and dielectric properties, *J. Sol-Gel Sci. Technol.* 86 (2018) 104–111. <https://doi.org/10.1007/s10971-018-4613-2>.
- [7] W. Shu-Yu, H. Wen-Zhi, L. Chang, L. Guang-Ming, Z. Fei-Er, Characterizations and preparation of Mg(OH)₂ nanocrystals through ultrasonic–hydrothermal route, *Res. Chem. Intermed.* 42 (2016) 4135–4145. <https://doi.org/10.1007/s11164-015-2264-2>.
- [8] J. Zheng, W. Zhou, Solution-phase synthesis of magnesium hydroxide nanotubes, *Mater. Lett.* 127 (2014) 17–19. <https://doi.org/10.1016/j.matlet.2014.04.076>.
- [9] A. Alamdari, R.M. Rahimpour, N. Esfandiari, E. Nourafkan, Kinetics of magnesium hydroxide precipitation from sea bittern, *Chem. Eng. Process. Process Intensif.* 47 (2008) 215–221. <https://doi.org/10.1016/j.cep.2007.02.012>.
- [10] S. Yousefi, B. Ghasemi, M. Tajally, PEG-assisted synthesis and formation mechanism of Mg(OH)₂ nanostructures using natural brine, *Appl. Phys. A Mater. Sci. Process.* 126 (2020). <https://doi.org/10.1007/s00339-020-03814-w>.
- [11] M. Turek, W. Gnot, Precipitation of Magnesium Hydroxide from Brine, *Ind. Eng. Chem. Res.* 34 (1995) 244–250. <https://doi.org/10.1021/ie00040a025>.
- [12] A. Pilarska, M. Wysokowski, E. Markiewicz, T. Jesionowski, Synthesis of magnesium hydroxide and its calcinates by a precipitation method with the use of magnesium sulfate and poly(ethylene glycols), *Powder Technol.* 235 (2013) 148–157. <https://doi.org/10.1016/j.powtec.2012.10.008>.
- [13] J.P. Hsu, A. Nacu, Preparation of submicron-sized Mg(OH)₂ particles through precipitation, *Colloids Surfaces A Physicochem. Eng. Asp.* 262 (2005) 220–231. <https://doi.org/10.1016/j.colsurfa.2005.04.038>.
- [14] H. Wu, B. Luo, C. Gao, L. Wang, Y. Wang, Q. Zhang, Synthesis and size control of monodisperse magnesium hydroxide nanoparticles by microemulsion method, *J. Dispers. Sci. Technol.* 41 (2020) 585–591. <https://doi.org/10.1080/01932691.2019.1594887>.
- [15] X. Li, C. Ma, J. Zhao, Z. Li, S. Xu, Y. Liu, Preparation of magnesium hydroxide nanoplates using a bubbling setup, *Powder Technol.* 198 (2010) 292–297. <https://doi.org/10.1016/j.powtec.2009.11.024>.
- [16] D. Wang, C. Song, Z. Hu, Synthesis of Mono-Dispersed Mg(OH)₂ Nanoflakelets, *J. Dispers. Sci. Technol.* 29 (2008) 1010–1012. <https://doi.org/10.1080/01932690701810011>.
- [17] D. La Corte, F. Vassallo, A. Cipollina, M. Turek, A. Tamburini, G. Micale, A novel ionic exchange membrane crystallizer to recover magnesium hydroxide from seawater and industrial brines, *Membranes (Basel)*. 10 (2020) 1–14. <https://doi.org/10.3390/membranes10110303>.
- [18] F. Vassallo, C. Morgante, G. Battaglia, D. La Corte, M. Micari, A. Cipollina, A. Tamburini, G.

- Micale, A simulation tool for ion exchange membrane crystallization of magnesium hydroxide from waste brine, *Chem. Eng. Res. Des.* (2021). <https://doi.org/10.1016/j.cherd.2021.07.008>.
- [19] F. Vassallo, D. La Corte, N. Cancilla, A. Tamburini, M. Bevacqua, A. Cipollina, G. Micale, A pilot-plant for the selective recovery of magnesium and calcium from waste brines, *Desalination*. 517 (2021). <https://doi.org/10.1016/j.desal.2021.115231>.
- [20] S. Bhandarkar, R. Brown, J. Estrin, Studies in rapid precipitation of hydroxides of calcium and magnesium, *J. Cryst. Growth*. 97 (1989) 406–414. [https://doi.org/10.1016/0022-0248\(89\)90222-4](https://doi.org/10.1016/0022-0248(89)90222-4).
- [21] D.J. Gunn, M.S. Murthy, M.S. Murthy, Kinetics and mechanisms of precipitations, *Chem. Eng. Sci.* 27 (1972) 1293–1313. [https://doi.org/10.1016/0009-2509\(72\)80105-2](https://doi.org/10.1016/0009-2509(72)80105-2).
- [22] Q. Yuan, Z. Lu, P. Zhang, X. Luo, X. Ren, T.D. Golden, Study of the synthesis and crystallization kinetics of magnesium hydroxide, *Mater. Chem. Phys.* 162 (2015) 734–742. <https://doi.org/10.1016/j.matchemphys.2015.06.048>.
- [23] A.E. Nielsen, O. Söhnel, Interfacial tensions electrolyte crystal-aqueous solution, from nucleation data, *J. Cryst. Growth*. 11 (1971) 233–242. [https://doi.org/10.1016/0022-0248\(71\)90090-X](https://doi.org/10.1016/0022-0248(71)90090-X).
- [24] A. Packter, The Rapid Precipitation of Magnesium Hydroxide from Aqueous Solutions: Analysis of Nucleation and Crystal Growth Kinetics, Final Nucleus Numbers and Primary Crystal Sizes, *Cryst. Res. Technol.* 20 (1985) 329–336. <https://doi.org/10.1002/crat.2170200307>.
- [25] V.S. Shirure, A.S. Pore, V.G. Pangarkar, Intensification of precipitation using narrow channel reactors: Magnesium hydroxide precipitation, *Ind. Eng. Chem. Res.* 44 (2005) 5500–5507. <https://doi.org/10.1021/ie049248d>.
- [26] X. Song, S. Sun, D. Zhang, J. Wang, J. Yu, Synthesis and characterization of magnesium hydroxide by batch reaction crystallization, *Front. Chem. Sci. Eng.* 5 (2011) 416–421. <https://doi.org/10.1007/s11705-011-1125-9>.
- [27] C.Y. Tai, C. Te Tai, M.H. Chang, H.S. Liu, Synthesis of magnesium hydroxide and oxide nanoparticles using a spinning disk reactor, *Ind. Eng. Chem. Res.* 46 (2007) 5536–5541. <https://doi.org/10.1021/ie060869b>.
- [28] H. Shen, Y. Liu, B. Song, Preparation and characterization of magnesium hydroxide nanoparticles in a novel impinging stream-rotating packed bed reactor, *J. Chem. Eng. Japan*. 49 (2016) 372–378. <https://doi.org/10.1252/jcej.15we093>.
- [29] G. Nichols, S. Byard, M.J. Bloxham, J. Botterill, N.J. Dawson, A. Dennis, V. Diart, N.C. North, J.D. Sherwood, A review of the terms agglomerate and aggregate with a recommendation for nomenclature used in powder and particle characterization, *J. Pharm. Sci.* 91 (2002) 2103–2109. <https://doi.org/10.1002/jps.10191>.

- [30] M. Roelands, J. Derksen, J. ter Horst, H. Kramer, P. Jansens, An analysis of mixing in a typical experimental setup to measure nucleation rates of precipitation processes, *Chem. Eng. Technol.* 26 (2003) 296–303. <https://doi.org/10.1002/ceat.200390045>.
- [31] C. Lindenberg, J. Schöll, L. Vicum, M. Mazzotti, J. Brozio, Experimental characterization and multi-scale modeling of mixing in static mixers, *Chem. Eng. Sci.* 63 (2008) 4135–4149. <https://doi.org/10.1016/j.ces.2008.05.026>.
- [32] S. Romano, G. Battaglia, S. Bonafede, D. Marchisio, M. Ciofalo, A. Tamburini, A. Cipollina, G. Micale, Experimental Assessment of the Mixing Quality in a Circular Cross-sectional T-shaped Mixer for the Precipitation of Sparingly Soluble Compounds, in: *Chem. Eng. Trans.*, 2021: pp. 1165–1170. <https://doi.org/10.3303/CET2186195>.
- [33] D. Bothe, C. Stemich, H.J. Warnecke, Fluid mixing in a T-shaped micro-mixer, *Chem. Eng. Sci.* 61 (2006) 2950–2958. <https://doi.org/10.1016/j.ces.2005.10.060>.
- [34] F. Storti, F. Balsamo, Particle size distributions by laser diffraction: Sensitivity of granular matter strength to analytical operating procedures, *Solid Earth*. 1 (2010) 25–48. <https://doi.org/10.5194/se-1-25-2010>.
- [35] M. Ryzak, A. Bieganski, Methodological aspects of determining soil particle-size distribution using the laser diffraction method, *J. Plant Nutr. Soil Sci.* 174 (2011) 624–633. <https://doi.org/10.1002/jpln.201000255>.
- [36] M. Sperazza, J.N. Moore, M.S. Hendrix, High-resolution particle size analysis of naturally occurring very fine-grained sediment through laser diffractometry, *J. Sediment. Res.* 74 (2004) 736–743. <https://doi.org/10.1306/031104740736>.
- [37] M.M.M.G.P.G. Mantilaka, H.M.T.G.A. Pitawala, D.G.G.P. Karunaratne, R.M.G. Rajapakse, Nanocrystalline magnesium oxide from dolomite via poly(acrylate) stabilized magnesium hydroxide colloids, *Colloids Surfaces A Physicochem. Eng. Asp.* 443 (2014) 201–208. <https://doi.org/10.1016/j.colsurfa.2013.11.020>.
- [38] D.L. Marchisio, L. Rivautella, A.A. Barresi, Design and scale-up of chemical reactors for nanoparticle precipitation, *AIChE J.* 52 (2006) 1877–1887. <https://doi.org/10.1002/aic.10786>.
- [39] M. Kucher, D. Babic, M. Kind, Precipitation of barium sulfate: Experimental investigation about the influence of supersaturation and free lattice ion ratio on particle formation, *Chem. Eng. Process. Process Intensif.* 45 (2006) 900–907. <https://doi.org/10.1016/j.cep.2005.12.006>.
- [40] H.C. Schwarzer, W. Peukert, Combined experimental/numerical study on the precipitation of nanoparticles, *AIChE J.* 50 (2004) 3234–3247. <https://doi.org/10.1002/aic.10277>.
- [41] K. Tong, X. Song, G. Xiao, J. Yu, Colloidal processing of Mg(OH)₂ aqueous suspensions using sodium polyacrylate as dispersant, *Ind. Eng. Chem. Res.* 53 (2014) 4755–4762. <https://doi.org/10.1021/ie5002857>.
- [42] C. Henrist, J.P. Mathieu, C. Vogels, A. Rulmont, R. Cloots, Morphological study of magnesium

- hydroxide nanoparticles precipitated in dilute aqueous solution, *J. Cryst. Growth.* 249 (2003) 321–330. [https://doi.org/10.1016/S0022-0248\(02\)02068-7](https://doi.org/10.1016/S0022-0248(02)02068-7).
- [43] N.G. Özcan-Taşkin, G. Padron, A. Voelkel, Effect of particle type on the mechanisms of break up of nanoscale particle clusters, *Chem. Eng. Res. Des.* 87 (2009) 468–473. <https://doi.org/10.1016/j.cherd.2008.12.012>.
- [44] A. Mersmann, *Crystallization Technology Handbook*, CRC Press, 2010.
- [45] P.H. Karpiński, J. Bałdyga, Precipitation Processes, in: *Handb. Ind. Cryst.*, Cambridge University Press, 2019: pp. 216–265. <https://doi.org/10.1017/9781139026949.008>.
- [46] G. V. Lowry, R.J. Hill, S. Harper, A.F. Rawle, C.O. Hendren, F. Klaessig, U. Nobbmann, P. Sayre, J. Rumble, Guidance to improve the scientific value of zeta-potential measurements in nanoEHS, *Environ. Sci. Nano.* 3 (2016) 953–965. <https://doi.org/10.1039/c6en00136j>.
- [47] J.X. Lin, L. Wang, Adsorption of dyes using magnesium hydroxide-modified diatomite, *Desalin. Water Treat.* 8 (2009) 263–271. <https://doi.org/10.5004/dwt.2009.786>.
- [48] G.A. Parks, The Isoelectric Points of Solid Oxides, Solid Hydroxides, and Aqueous Hydroxo Complex Systems, *Chem. Rev.* 65 (1965) 177–198. <https://doi.org/10.1021/cr60234a002>.
- [49] V.A. Phillips, J.L. Kolbe, H. Opperhauser, Effect of pH on the growth of Mg(OH)₂ crystals in an aqueous environment at 60°C, *J. Cryst. Growth.* 41 (1977) 228–234. [https://doi.org/10.1016/0022-0248\(77\)90050-1](https://doi.org/10.1016/0022-0248(77)90050-1).
- [50] G.S. Smith, Human color vision and the unsaturated blue color of the daytime sky, *Am. J. Phys.* 73 (2005) 590–597. <https://doi.org/10.1119/1.1858479>.
- [51] X. Pan, Y. Wang, Z. Chen, D. Pan, Y. Cheng, Z. Liu, Z. Lin, X. Guan, Investigation of antibacterial activity and related mechanism of a series of nano-Mg(OH)₂, *ACS Appl. Mater. Interfaces.* 5 (2013) 1137–1142. <https://doi.org/10.1021/am302910q>.